Wear 556-557 (2024) 205515

Contents lists available at ScienceDirect

Wear

journal homepage: www.elsevier.com/locate/wear

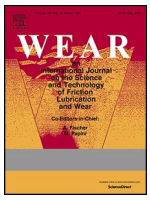

Study on the wear characteristics of a 3D printed tool in flat lapping of Al_2O_3 ceramic materials

Mariusz Deja [a,*], Dawid Zieliński [a], Sisay Workineh Agebo [b]

[a] Faculty of Mechanical Engineering and Ship Technology, Department of Manufacturing and Production Engineering, Institute of Machine and Materials Technology, Gdańsk University of Technology, Gabriela Narutowicza Street 11/12, 80 - 233, Gdańsk, Poland
[b] Doctoral School at Gdańsk University of Technology, Gabriela Narutowicza Street 11/12, 80 - 233, Gdańsk, Poland

ARTICLE INFO

Keywords:
Tool wear
Abrasive machining
Single-sided lapping
Rapid tooling
Selective laser sintering
Ceramic materials

ABSTRACT

Widespread and popular use of ceramic products in various industry sectors necessitates the search for methods of their efficient processing. Lapping technology, which enables obtaining high dimensional and shape accuracy and high surface flatness, is one of the basic methods of finishing hard and brittle technical ceramics with a porous structure. This study analyzed the characteristics and wear value of an SLS-printed abrasive tool intended for single-sided lapping of Al_2O_3 technical ceramics. As earlier research demonstrated, introduction of a 3D printed lapping plate by selective laser sintering (SLS), leads to a significant development in the field of precision machining technology. This method showed not only efficient machining performance on oxide technical materials, but was also characterized by relatively low abrasive wear. Straightness errors were evaluated with the use of a least-squares method (LSQ) and minimum zone method based on control line rotation scheme (CLRS). The proposed model proved the experimental results by identifying a similar location of a higher contact density on the lapping tool, where this location is expected to be the one for bigger wear. Surface topography of the lapping tool depends on the tool wear intensity and as a consequence on its shape error. An SLS-printed lapping plate, by obtaining good technological effects, revealed its potential ability in machining hard and brittle technical ceramics.

1. Introduction

Nowadays, ceramic materials are widely used in many industrial sectors, e.g. in the electronics industry, mainly in the production of silicon and sapphire wafers or sapphire glass panes used in electronic devices such as smartphones or light emitting diode (LED). Dynamic development of the electronics industry results in increased requirements for electronics substrates. Characteristic properties of ceramic materials associated with high hardness and porous structure require the use of appropriate finishing operations. Typically used abrasive methods for this type of material are chemical mechanical polishing (CMP) [1,2] and single or double-sided lapping [3–5].

Lapping technology is commonly and widely used for obtaining very fine surface finishes, minimal subsurface damage, as well as high dimensional and shape (flatness) accuracy of metallic and non-metallic materials, including hard and brittle ceramics characterized by porous structure [6–10]. This method can effectively remove or reduce waviness and subsurface damage caused by previous operations [3,8]. Although the lapping technology has been known and developed for many years, it is still the subject of many contemporary research works. Currently, various lapping methods are used e.g. slurry free or free abrasive lapping, when abrasive particles are applied directly to a lapping wheel, as during grinding [11]. Although the lapping technology is performed using relatively simple technological means, it requires a lot of experience and knowledge in the selection of appropriate tools, type of abrasive slurry and machining parameters [12–14]. In practice, obtaining characteristic lapping technological effects depends on a large number of variables. In addition to the controlled input factors associated with the workpiece, the abrasive tool and slurry employed, and the machining process parameters [15,16], authors of the papers [17,18] also indicated a group of uncontrolled factors. These can be exemplified by the interferences that occur during machining, such as system vibrations and environmental temperature, which have an adverse effect on the process quality and machining results. The application of modern computer control techniques and simulations e.g. in high speed grinding or polishing, which enable the control of particular process parameters,

* Corresponding author.
E-mail address: mariusz.deja@pg.edu.pl (M. Deja).

https://doi.org/10.1016/j.wear.2024.205515
Received 24 January 2024; Received in revised form 17 June 2024; Accepted 25 July 2024
Available online 26 July 2024

can improve process accuracy and efficiency as well as quality of machined workpiece [19–21].

One of the most important lapping factors directly influencing the dimensional and shape accuracy of the workpiece is the plate shape. As a result of the interaction of the abrasive grains, the lapping plate gradually wears, which also changes the shape of its external surface and, in consequence, results in flatness errors. In the case of standard lapping with cast iron plates, it is therefore possible for the tool to take the following shape errors: convex, concave or axial runout [15,22]. However, too frequent conditioning operations result in a significant increase in production cost and a decrease in process efficiency [23,24]. Therefore, it is very important to carry out the wear characteristics of the lapping plate. Due to the fact that the active surface of the tool is simultaneously the machining datum surface, there is a very close correlation between the lapping disc and the machined workpiece flatness errors [5]. For this reason, it is necessary to reduce the amount of tool wear, especially the wear of lapping plates made of soft materials.

One of the major factors determining tool wear are the kinematic conditions. Authors of the paper [25] studied an unconventional single-sided lapping system. It was found that introducing more additional and controlled movements of a conditioning ring can change the density of grains trajectories and, in consequence, reduce the occurrence of more uneven wear compared to conventional lapping method. Many researchers have also been studying the effect of the lapping plate shape on the shape accuracy of the workpiece made of sapphire and silicon wafers. In research performed by Lee et al. [4] on sapphire wafer, authors were focused on the effect of platen shape on TTV (total thickness variation) generation in single-sided lapping of sapphire wafer. Changes of platen shape change pressure distribution on wafer and in consequence result in different material removal rate. As presented in Ref. [26] convex workpieces should be obtained on the concave platen, and concave workpieces can be obtained on the convex platen. Numerous research focus on the amount of wear and the speed of the lapping wheel based on the lapping trajectory [27,28], whereas it is observed in numerous articles [29–31], that lapping trajectory has a significant impact on processing and machined workpiece quality. Uneven distribution of the lapping trajectory leads to uneven wear on the lapping wheel, resulting in its uneven surface and the surface shape accuracy of the machined workpiece [16,32]. Lai et al. [29] proposed the double-sided lapping wear model of the lapping wheel surface according to the distribution density of the trajectory. The calculation results have been verified by experimental data of sapphire slices double-sided lapping. In the study of Barylski and Deja [5], a model for the tool wear prediction is developed, which can be used for both standard lapping and grinding with single or double-disc lapping kinematics. Proposed model based on the trajectory distribution, motion velocity and acceleration of the workpiece was then used to compare the simulation results with experimental data obtained in double-disc lapping of silicon wafers. The experimental results were consistent with tendency obtained from the simulation tests.

Ensuring uniform wear of the tool enabling greater accuracy of the shape of the processed surfaces, as well as improving the efficiency of the machining process itself, necessitates the development of innovative abrasive tools. A review of selected scientific works indicates the growing importance of additive technologies, the enormous potential of which is used to build, among others, resin abrasive tools, including lapping discs [33–36]. Methods based on laser, like stereolithography (SLA) or UV light-curing resins, as well as SLS using polyamide powder, enable the relatively fast and low-cost fabrication of soft abrasive tools. Considering the cutting mechanism, the abrasive grains penetrate into the tool structure, helping to reduce the roughness of the workpieces. Additive methods based on metal powders allow the fabrication of tools with significantly higher mechanical properties, mainly used as grinding wheels working in various conditions. The fabrication and post-processing costs of the metal-bonded abrasive tools are much higher compared to non-metal tools. Currently, especially 3D printing powder technologies, including the SLS method, enable the production of fully functional objects with complex geometries, including the parts for the tool industry - Rapid Tooling [37–39]. The results of lapping selected materials, including hard and brittle technical ceramics, presented in the literature with the use of resin abrasive tools indicate their great potential. In the research studies presented in [40,41], lapping is performed on technical ceramics and sapphire samples using resin lapping discs containing diamond grains. The obtained results of selected experimental tests indicated a lower roughness of the treated surfaces and a higher material removal rate compared to the conventional lapping process with a cast iron plate. Despite obtaining positive technological effects, one of the main disadvantages of printed abrasive tools is their high wear during processing, which limits their wider industrial application. As reported in Ref. [42], the wear value of the resin lapping disc made using the SLA stereolithography method during glass processing was more than twice the size of the material being cut.

In the previous research study, it was proposed to use SLS technology to create a lapping disc to be used as an abrasive tool. Even after machining of hard technical ceramics, the tool showed remarkable efficiency and very little abrasive wear [43]. However, the literature survey indicates the necessity of research to characterize the wear of lapping tools fabricated with powder-based 3D printing technologies becoming a promising solution for developing new tools for abrasive finishing. In this study, the wear of an SLS-fabricated lapping tool made of polyamide PA2200 powder is assessed using a non-contact type 3D optical profilometer and a contact type digital sensor. Straightness errors were evaluated by employing a least-square and minimum zone methods. Furthermore, a model for determining the contact density along the radial axis of the lapping segments was adopted.

Table 1
Recent research studies in lapping tool wear.

Types of tools	Workpieces	Measurement methods	References
Optical glassgrades K8 and LK5	Lithium niobate single crystals	Form tester (MarForm MMQ 400)	(Muratov et al., 2021)
Solid cast iron	Tellurium copper	Lapmaster flatness gauge	(Barylski & Piotrowski, 2019)
Solid cast iron	cBN segments	Electronic depth gauge	(Macerol et al., 2022)
Three hydrophilic FA pads With W50 SCD, W10 SCD, and AD abrasives	Fused quartz	SEM - image particle size analyzer	(Wang et al., 2019)
Fixed AD abrasive pads and fixed single crystal diamond abrasive pad	Sapphire wafers	SEM and energy dispersive spectrometer	(Chen et al., 2020)
Two FA diamond lapping plate with different mechanical properties	Sapphire wafers	SEM	(Xiong et al., 2022)
Metal (Al, CU, Sn)–resin platen with diamond slurry	Sapphire	FE-SEM	(Kim et al., 2015)
Methacrylate photopolymer resin printed with 50 μm and 100 μm layer thickness	Schott glass discs	Weighing	(Williams & Carolina, 2015)
Double sided lapping wheel with abrasive particle 240 B4C(61 μm)	c-plane sapphire slices	Surface profilometer	(Lai et al., 2019)
FA diamond abrasive pad (Trizact™ pad, 9 μm abrasive size, 3 M, USA)	Fused quartz glass	SEM micrographs	(Bin et al., 2020)

2. Overview of related research studies

The results of related research studies on lapping tool wear vary based on the exact experimental setting and materials employed. Table 1 summarises some of the most recent related research investigations. These findings emphasise the effect of variables such as lapping tool diameter, kinematic parameters, grit characteristics, and load on lapping tool wear.

Muratov et al. [44] carried out an experimental research with a lapping tool made of optical glass grades K8 and LK5 with a diameter of 200 mm for lapping lithium niobate single crystal samples. They used a method form tester (MarForm MMQ 400) to assess tool wear, and the results demonstrate that local tool wear vary on the radius of the lapping tool, with greatest wear recorded at greater radii. In the study presented in Ref. [25], cast iron lapping tool material were utilized for lapping tellurium copper, and a Lapmaster flatness gauge to analyze lapping tool wear. According to the findings of the experimental investigation, optimizing kinematic parameters and adding extra movements to the conditioning ring can result in more uniform wear of the lapping plate. An electronic depth gauge was used to measure the wear rates of cBN segments lapping with a solid cast iron lapping tool, and the results show that grit toughness and abrasive wear resistance of the lapping pad material are important factors in determining wear rates, with higher AR grits wearing faster than lower AR grit [45].

Wang et al. compared in Ref. [46] three hydrophilic fixed abrasive (FA) pads, one with W50 SCD abrasives, one with W10 SCD abrasives, and one with AD abrasives, for lapping of fused quartz samples. The lapping tool wear was studied using a scanning electron microscope (SEM) and an image particle size analyzer. According to the findings, a greater debris increases the wear rate of the pad matrix, and the FA pad embedded with AD has greater wear resistance than the W10 SCD and W50 SCD. Chen et al. [47] used a SEM and an energy dispersive spectrometer to measure tool wear while lapping sapphire wafer samples with a lapping tool of fixed agglomerated diamond abrasive pads and fixed single crystal diamond abrasive pads. According to the comparison study, FAD had less tool wear than SCD.

The SEM analysis from the research revealed that the lapping plates mostly suffer from abrasive wear, bond fracture, abrasive breaking, and abrasive peeling off during the lapping of sapphire wafer samples using a lapping tool of two fixed-abrasive diamond lapping plates with varying mechanical properties [48]. A metal (Al, CU, Sn)-resin platen was employed with diamond slurry during the lapping of a sapphire workpiece, and the lapping tool wear was analyzed using FE-SEM, and plates with abrasive wear, abrasive flattening, and abrasive peeling off were detected [49]. In the study of [42], a lapping tool methacrylate photopolymer resin printed with 50 μm and 100 μm layer thickness was utilized for lapping Schott glass discs, and the wear of the lapping tool was assessed by weighing on the Ohaus Adventure Pro balance. The tool wear rates for the 100 μm and 50 μm layer tools were comparable, but the 50 μm layer tool was 74 % more successful at removing material from the glass sample. A double sided lapping wheel with abrasive particle 240 B4C (61 μm) and a sample of c-plane sapphire slices were used to investigate the wear of the tool by employing a surface profilometer for observing the tool wear, and the result shows that the inner area of lapping plate is convex, and the central area is concave, and the wear increases with increased lapping speed [50]. Additionally, lapping speed and load also play a significant role in determining the degree of wear. Bin et al. [51] studied the wear of lapping tool fixed diamond abrasive pad (Trizact™ pad, 9 μm abrasive size, 3 M, USA) during lapping fused quartz glass. SEM and micrographs were used to analyze the wear of lapping tool and the result showed that a lapping tool pad surface was stable after 120 s lapping with 25 N load but worn out for 30 N load.

Extensive studies have been undertaken on conventional lapping tool materials, which aided in the advancement of the modern lapping industries. At the moment, additive manufacturing is playing an important part in the production of numerous sophisticated machine tools using layer-by-layer manufacturing processes. A literature query, however, reveals that no models were employed to predict and characterize the wear of abrasive tools manufactured using 3D printing powder technologies. Moreover, further research is required to understand the intricate mechanisms underlying lapping tool wear and to discover effective ways for extending tool life and enhancing performance. Lapping tools with uniform tool wear are critical for lowering production costs, improving machining workpiece quality, and increasing productivity. This study mainly investigates and explores the wear characteristics of a 3D printed abrasive tool in single-sided flat lapping of a difficult to cut material, Al_2O_3 ceramic material.

3. Experimental setup and investigations

Experimental tests on the lapping of Al_2O_3 samples were carried out on a prototype machine tool design, which enables lapping and grinding processes to be carried out with the kinematics of lapping flat surfaces. The device has two independent and programmable drive units of the lapping disc and the guide ring, which enables machining processes to be carried out using various kinematic conditions. The printed prototype abrasive segments were attached to the metal body of the device using 32 metric screws, as shown schematically in Fig. 1a. The process of printing the lapping disc segments was carried out on an industrial EOS Formiga P100 3D printer operating in SLS technology using a set of parameters, type of material and post-processing specified in Table 2. Table 3 provides the most important mechanical and physical properties of the polyamide used. Another significant modification of the research device used was the lack of contact of the guide ring with the disc surface as shown in Fig. 1b, which results in less wear of the tool made of sintered SLS polyamide powder.

The experimental tests were divided into specific lengths of tests, which were carried out using a set of parameters given in Table 4. As presented in Ref. [43], the adopted set of parameters enabled an effective processing of Al_2O_3 samples and a significant reduction in the roughness and waviness parameters of their surface. Moreover, two sets of lapping discs were used in these experimental tests, for which measurements of the wear and shape errors were made.

In order to quantitatively estimate the wear value of lapping discs and determine their flatness error in individual processing stages, the shape of the active surface of the tools was analyzed in relation to the initial shape before the start of machining. Measurements were made using a digital measurement sensor from Mitutoyo with a reading accuracy of ±0.001 mm, which was attached to the stand with a strong electromagnet. Prototype abrasive segments attached with screws to a metal body, forming a flat surface of the lapping disc, were placed in the rigid body of the Carl Zeiss Jena universal microscope and immobilized by pressing with clamping claws on both sides. A view of the stand intended for measuring shape errors of a prototype lapping disc along with an indication of its key elements is presented in Fig. 2.

Measurements were taken along the centerline of each abrasive segment in the radial direction at specific points and according to a polar grid strategy. As a result, 8 radial profiles were obtained, which were determined from 14 measurement points (112 measurements in total) and assuming a constant distance of d = 10 mm between them – Fig. 3. After completing the measurement of individual abrasive segments, the digital sensor was lifted and the lapping disc was rotated by an angle of 45° to measure the next abrasive segment. The collected data were then used to create charts showing the total variability of the flatness of the prototype lapping disc and a model illustrating the actual shape of the tool disc. The obtained profiles (plate flatness profiles, radial sections) for each of the tools were then used to determine the amount of their wear and the resulting straightness errors.

Moreover, surface topography measurements of Al_2O_3 samples and selected SLS-printed segments of the lapping wheel were carried out by 3D optical profilometer Sensofar S neox in the measurement points

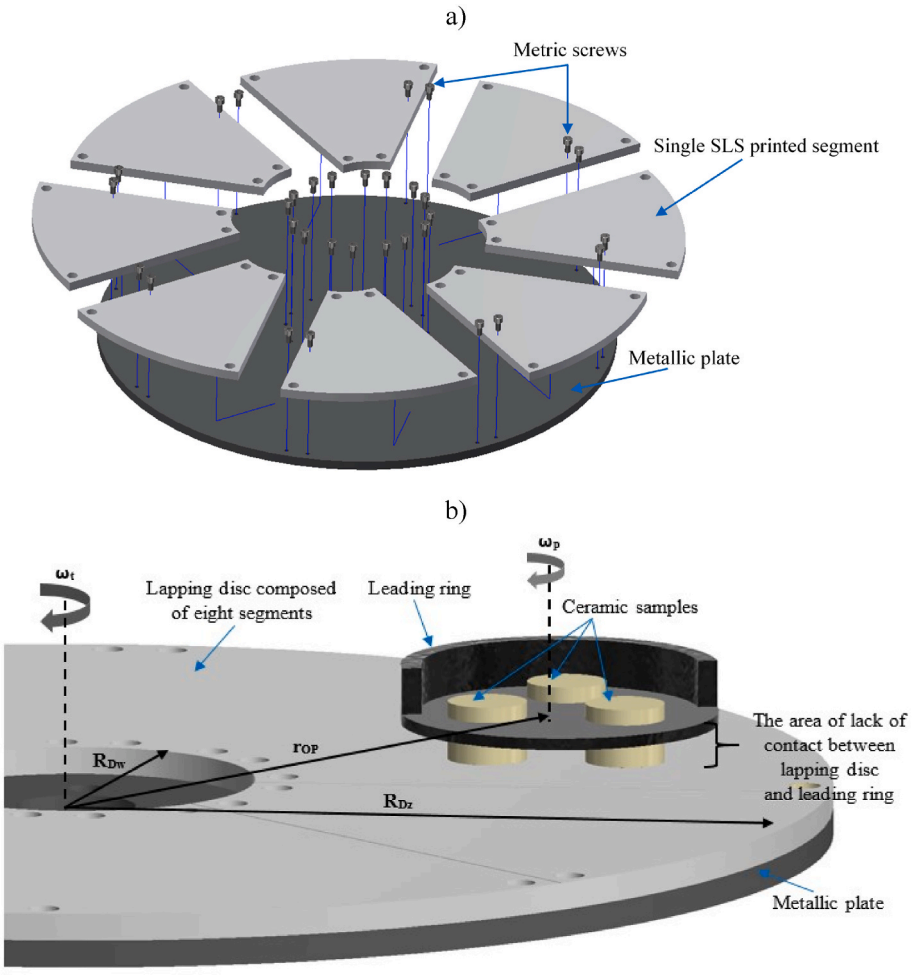

Fig. 1. Schematic drawing of the lapping disc composed of eight abrasive segments mounted on a metallic plate: a) general view of the lapping disc, b) the area of lack of contact between lapping disc and leading ring (explanation of symbols given in Table 4).

Table 2
Additive process parameters used for printing lapping tools.

3D printing system	Powder material	
EOS Formiga P100	Polyamide PA2200	
Process parameters	**Values**	**Unit**
Thickness of a single layer of a laid material	100	μm
Power of a CO_2 laser	30	W
Printing speed	10	mm/s
Printing resolution	0.005	mm
Length of a laser beam	10.6	μm
Printing orientation	vertical	–
Post processing methods		
Basic post processing including sandblasting and final cleaning from unsintered polyamide particles with the use of compressed air		

Table 3
Selected mechanical and physical properties of the polyamide PA2200 [52].

Tensile modulus	Tensile strength	Flexural modulus (23 °C)	Shore D hardness (15 s)	Density after laser sintering
1650 MPa (X, Y, Z direction)	48 MPa (X, Y direction) 42 MPa (Z direction)	1500 MPa (X direction)	75	930 kg/m^3

indicated in Fig. 3 and according to the ISO 25178. For this purpose, the confocal technique with objective 20× magnification was used. The obtained surface topographies were then analyzed using SensoMAP Premium 9.1 software. The mass of the material loss from the ceramic samples was measured with the use of a laboratory balance with a resolution of 0.001 g.

4. Tool wear modeling

The intricate interaction between the lapping tool and the workpiece often determines the effectiveness of lapping processes in precision machining. It is essential to comprehend and measure this relationship in order to determine and predict tool wear. Normalized contact density is used to determine the intensity of contact between the workpiece and the tool by evaluating the ratio of the actual contact area between the lapping tool and the workpiece to the maximum or reference contact area. To determine the intensity of contact numerically, the surface of lapping plate is divided in to m_1 number of rings as shown in Fig. 4.

In this study, by offering a quantitative basis for evaluating the tool wear intensity during the lapping operation via the prism of MATLAB modeling and by adding normalized contact density to a lapping tool wear model, the lapping tool wear modeling calculations were made using the model presented in Ref. [5]. The length of trajectory traveled over the area of the ring k_u by the middle point P_{1i} of an elementary area A_{1i} during time $t = t_{kiu} - t_{piu}$ is determined by equation (1):

Table 4
Lapping conditions during experiments with the use of a SLS-printed tools.

Lapping plate			
Specification	Symbol	Value	Unit
Outer tool diameter	d_o	380	mm
Inner tool diameter	d_i	90	mm
Average initial surface roughness	*Sa*	15	μm
Lapping parameters			
Parameters	**Symbol**	**Value**	**Unit**
Unit pressure	p	12	kPa
Rotational speed of a lapping plate	n_t	120	min^{-1}
Rotational speed of a leading ring	n_w	60	min^{-1}
Duration of a single lapping test	t_t	120	min
Geometrical conditions of the simulation and experimental setup			
Parameters	**Symbol**	**Value**	**Unit**
Inner radius of the disc	R_{Dw}	45	mm
Outer radius of the disc	R_{Dz}	190	mm
Distance of the center of the guide ring from the center of the lapping disc	R	115	mm
Distance between the center of the guide ring and the center of the workpiece	r_{OP}	35	mm
Abrasive suspension			
Type and volume of abrasive suspension		Abrasive paste SD 28/20 (4 ml) Loose diamond grains D107 (2.5 ml)	
Lubricant type and PH		Machining oil, 5.60	
Lubricant flow rate	$\dot{Q}_{lub}$	0.5 ml/min	
Workpiece properties			
Ceramic type		Al_2O_3	
Vickers hardness	HV10	1100 MPa	
Sample shape and diameter	d_w	cylindrical with diameter 34 mm	
Initial height	h_{w0}	30 mm	
Average initial surface roughness	*Ra*	1.8 μm	

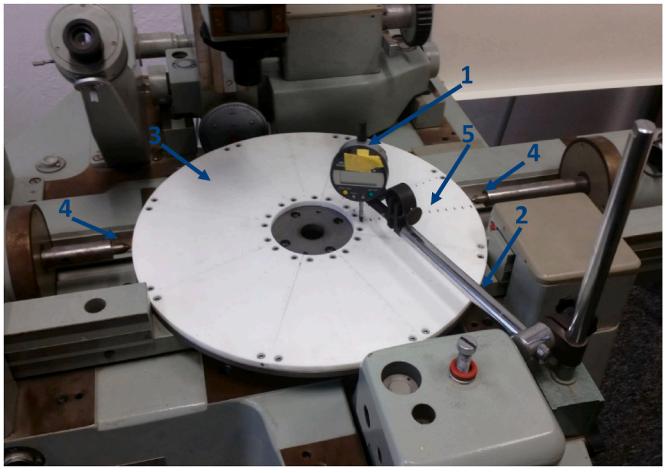

Fig. 2. Station for measuring the shape error of the lapping disc: 1 - digital sensor, 2 - stand with an electromagnet, 3 - tool disc screwed on to the metal body, 4 - mounting centers, 5 - measuring points.

$$\Delta s_{iu} = \int_{t_{piu}}^{t_{kiu}} v_{p_{1i}}(t)dt \tag{1}$$

As a function of the lap radius, the contact density between the workpiece and the tool's whole surface can be found for all n_4 elementary areas A_1:

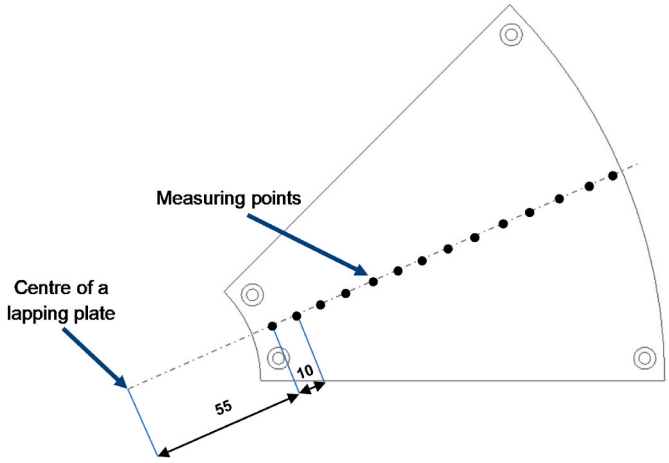

Fig. 3. Schematic drawing of measuring a single segment of a lapping plate.

$$d_g(R_D) = \lim_{m_1\to\infty}\left[A_1 . \lim_{n_4\to\infty}\sum_{i=1}^{n_4}\Delta s_{iu}\right]_{u=1,\ldots,m_1} \tag{2}$$

where:

A_1 – elementary workpiece area,

n_4 – total number of the workpiece elementary areas.

The specific ring area decreases with approach to the tool center, which increases the workpieces action for a given contact density. Differences in the tool ring regions are taken into account in the corrected contact density d_{gp}, by additional adjusting of equation (3) developed in [5], using an experimentally determined f coefficient related to the working conditions changing along the radius:

$$d_{gp}(R_D) = \lim_{m_1\to\infty}\left[\frac{A_1}{2\pi R_{ku} f \Delta w} . \lim_{n_4\to\infty}\sum_{i=1}^{n_4}\Delta s_{iu}\right]_{u=1,\ldots,m_1} \tag{3}$$

where:

$\Delta w = R_{kzu}$-R_{kwu}– width of the ring k_u,

f– coefficient determined experimentally. In one cycle time, the density for the radius $R_D = R$ contacting all elementary areas can be used to normalize the distribution of contact density:

$$d'g(R_D) = \frac{d_{gp}(R_D)}{d_{gp}(R)} \tag{4}$$

The distribution of contact density, or d_{gp} (R_D), can be used to estimate the degree of wear in a certain tool region. The spot with the highest contact density is anticipated to have a greater wear rate.

It was assumed that the wear of the tool depends on the contact intensity between the workpiece and the lapping tool. Calculations were made to determine the area where highest tool-workpiece intensity is located, with the parameters used in the experiment. Their result for normalized contact density is shown in Fig. 5, where the highest contact density is observed near to the inner radius of the tool rather than the outer, and bigger tool wear is expected at the radius of 90 mm. The tool wear modeling resulted in the investigation was proven by the tool wear determined experimentally using a digital measurement sensor from Mitutoyo and a surface profilometer.

5. Experimental results and discussion

5.1. Straightness analysis of a flat surface of the lapping plates

Straightness analysis of a flat surface of the prototype lapping plates was performed using a least-squares method *LSQ* and control line rotation scheme *CLRS* in accordance with the formula presented in the study

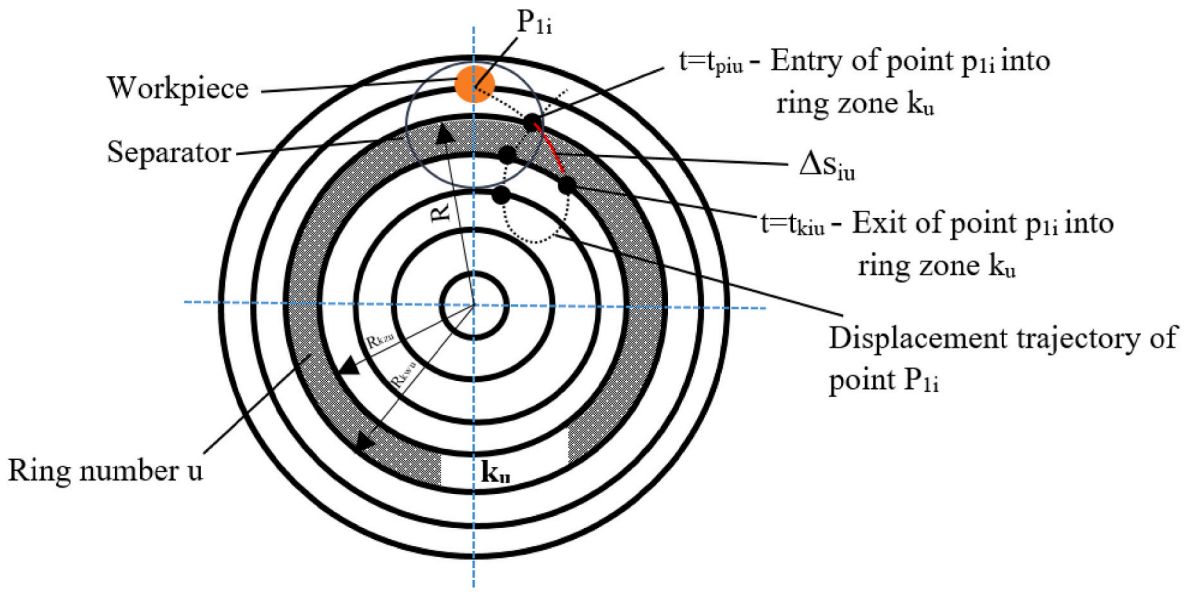

Fig. 4. Schematic illustration of lapping trajectory.

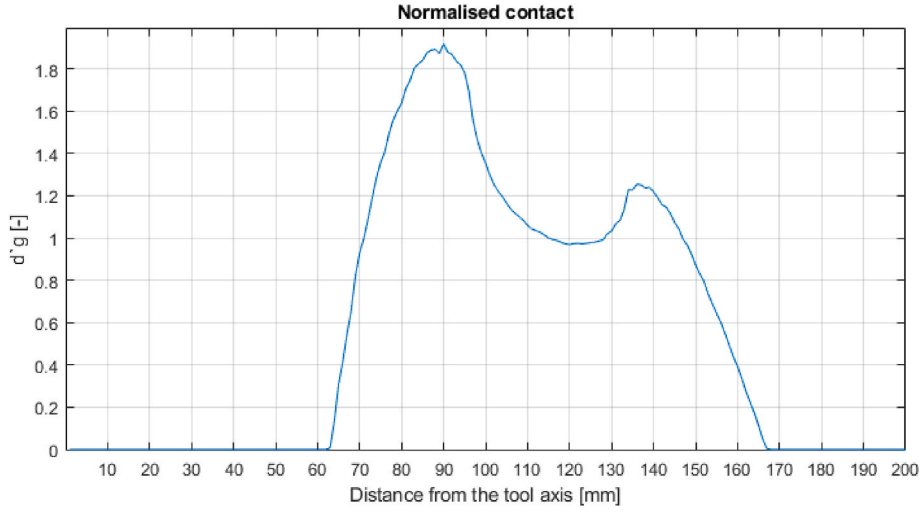

Fig. 5. Normalized contact density between the workpiece and the lapping tool calculated for the experiment setup and parameters.

[53]. According to the demonstrated procedure, the straightness deviations were determined before and after specific series of lapping. Additionally, using the *CLRS* method required constructing a 1-1 model based on the determined least-squares line (reference line) and then transforming it into the 2-1 model – Fig. 6. In the first step, the measurement data was used to create a basic profile of the tool marked in blue in Fig. 6. It was used as a base to define a least-squares line as a trend line, which was then used to determine the next two control lines parallel to it: upper passing through the highest point on the profile and lower passing through the lowest point on the profile. Finally, the straightness deviation determined by the *LSQ* method was the length of the segment ΔD_{LSQ} connecting the upper and lower control lines – Fig. 6a. Since the 1-1 model is associated with only two control points, determination of one additional point was performed to confirm the minimum zone solution procedure. The main step in constructing model 2-1 based on model 1-1 was to find an additional control point passing through the upper or lower control line. The creation of model 2-1 required the rotation of the upper control line around an additional control point i by an angle θ_i according to the rule described by relations equation (5) and equation (6):

$$\theta_i = \sin^{-1}\left(\frac{E_{mu} - E_i}{L_i}\right), \tag{5}$$

$$\theta_I = \text{minimum}\{\theta_i\} \tag{6}$$

where:

θ_i– the angle of rotation of the upper control line around the control point i,

E_{mu}– the deviation of the upper control point to the reference line,

E_i– the deviation of control point i to the reference line,

L_i – the distance from the upper control point to the control point i, or lower control line around an additional control point j by an angle θ_j according to the rule described by relations equation (7) and equation (8):

$$\theta_j = \sin^{-1}\left(\frac{E_{ml} - E_j}{j}\right), \tag{7}$$

$$\theta_J = \text{minimum}\{\theta_j\} \tag{8}$$

a)

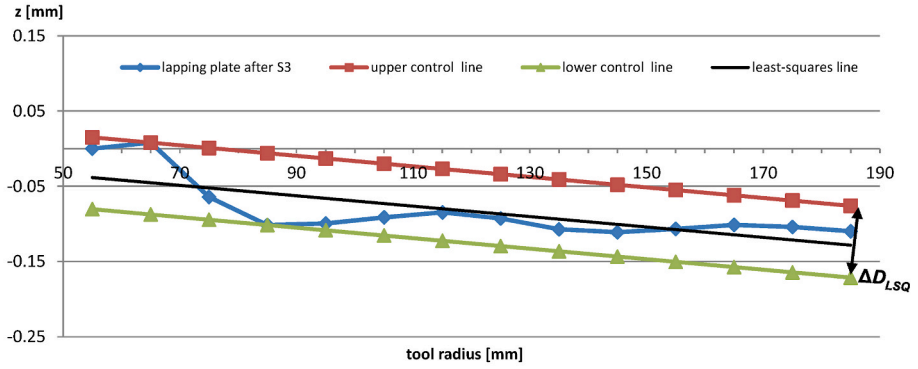

b)

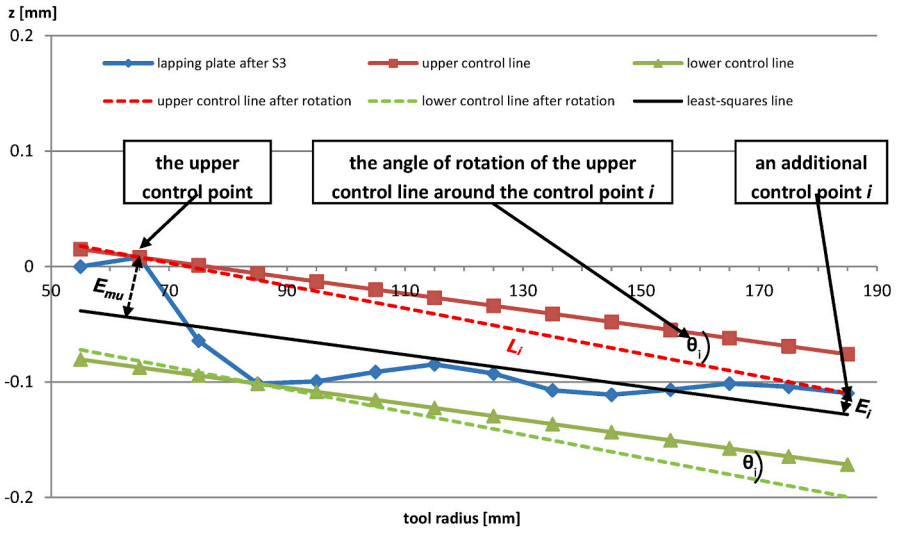

c)

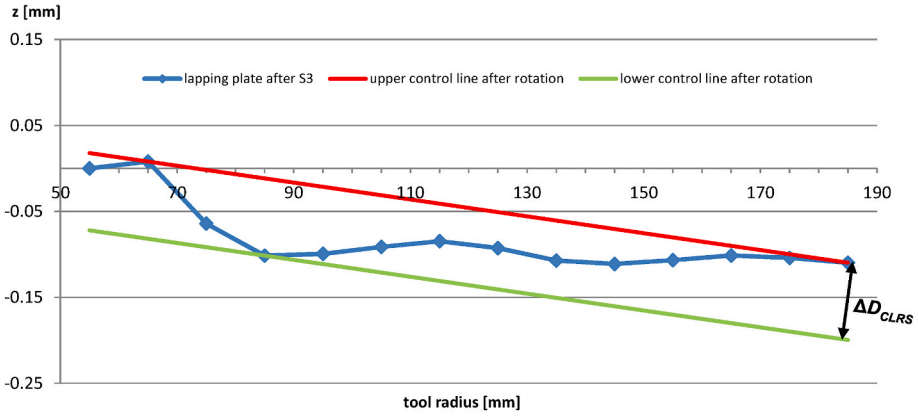

Fig. 6. The minimum zone searching: a) construction of the 1-1 model from the reference line – least-squares line, b) CLRS search from the 1-1 model to 2-1 model (rotations of the control lines around the corresponding control points according to *CLRS* rule); c) final results.

where:

θ_j– the angle of rotation of the lower control line around the control point j,

E_{ml}– the deviation of the lower control point to the reference line,

E_j– the deviation of control point j to the reference line,

L_j – the distance from the lower control point to the control point j.

Simultaneously, the criterion for selecting an additional control point i or j was the smaller value of the angle θ_i or θ_j. Both upper and lower control lines were then rotated by the indicated angle around the additional control point. Fig. 6b shows the transformation of model 1-1 to model 2-1 related to the selection of an additional control point i and the rotation of the control lines by an angle θ_i. This transformation of the model confirmed obeying the basis of the minimum zone solution, with the three points lying in an upper-lower-upper sequence. Finally, the

straightness deviation determined by the *CLRS* method was the length of the segment ΔD_{CLRS} as shown in Fig. 6c.

The calculated values of straightness deviations in terms of the least-squares and the minimum zone solutions were presented in Table 5.

The tested lapping wheels were characterized by relatively small straightness deviations. For both tools, the determined error values after the individual machining series were comparable, while their values increased with the lapping time. Meanwhile, the decreasing value of the coefficient of determination R^2 after subsequent machining series indicated an increasingly worse fit of the experimental data to the determined trend line and, consequently, a change in the shape of the flat surface of the lapping wheels. As seen in Tables 5 and in series 1 and 2, the values of R^2 (0.9132, 0.7829 – the tool no. 1, and 0.6954, 0.6661 – the tool no. 2) were bigger than for series 3, whereas the straightness deviations from both methods for the two lapping plates, i.e. for LSQ (0.061, 0.071 – the tool no.1, and 0.077, 0.082 – the tool no. 2) and for CLRS (0.056, 0.064 – the tool no. 1, and 0.051, 0.076 – the tool no. 2) were characterized under consistent deviation, indicating the uniformity of the wear mechanism. The value of R^2 in experimental series 3 was observed to decrease significantly from 0.7829 to 0.5504 and 0.6661 to 0.0907 for both lapping tools, respectively. The straightness deviation in both methods increased from 0.071 to 0.095 (LSQ) and 0.064 to 0.090 (CLRS) for tool 1, and from 0.082 to 0.095 (LSQ) and 0.076 to 0.095 (CLRS) for tool 2. This variation in the straightness and the lowest of R^2 values points out that the wear along the radial length of the lapping tool is not uniform. The largest straightness deviation was determined for lapping wheel no. 2 after total machining time of 840 min and amounted to just 0.095 mm for both methods. The significantly lower value of the coefficient of determination R^2 compared to the other series of lapping indicates the largest errors in the shape of the tool and its wear value. Both lapping tools in each series of experiments have experienced an increasing straightness deviation with the increase in lapping time. The tools were involved in progressive abrasive wear due to the interactions of the bodies involved in machining, mainly by abrasive particles rotating between the workpiece and the tool (three-body abrasion) or sliding after their embedment (two-body abrasion). The wear mechanism of lapping tools in each series of experiments and different contact intensity at specific areas of the wheel depending on the radius directly influenced the straightness deviations.

5.2. Topography of a flat surface of the lapping plate

Based on three-dimensional variations in a surface's height or depth, surface topography analysis is used to characterize the surface of a lapping tool. It is important in determining the no-, higher-, medium-, and less-contact zones based on the measured roughness magnitude Sa, as this could help to determine where the higher wear in the lapping tool is located.

The surface topography of a lapping plate segment #3 at chosen radii of 85, 125, and 175 mm is shown in Fig. 7. After 14 h of lapping the ceramic material Al_2O_3, surface topography investigation was carried out utilizing a non-contact type SENSOFAR surface profilometer with a 20× magnification scale.

As we look at the surface profilometer result for the third lapping tool segment in Fig. 8, we can see that the tool's surface has varied surface characteristics as we move from the inner to the outer radius of the tool. The tool's non-contact regions were found to be at 55, 175, and 185 mm in radius, with correspondingly higher Sa values of 14.38, 14.47, and 15.32 μm. The surface of the lap tool, with a radius of 65, 145, 155, and 165 mm, was found to have a lower contact area, with corresponding Sa values of 16.28, 9.41, 11.11, and 10.89 μm. The tool's medium contact area was measured with a radius of 115, 125, and 135 mm, with corresponding Sa values of 8.09, 13.79, and 7.34 μm. Near the inner lapping tool radius of 75, 85, 95, and 105 mm, a higher contact zone was noted along with a lower Sa value of 6.00, 5.32, 7.85, and 7.00 μm, respectively. When the observed data are examined, it can be found that the radius point 85 mm has the lowest Sa value and is found to be in a higher contact location. This is because the tool-workpiece friction at this radius is higher, which causes the tool surface to be machined during lapping and more wear occurs.

5.3. Technological effects

The experimental tests of single-sided flat lapping of technical ceramic samples were carried out using the same process parameters given in Table 4 for both lapping wheels. Fig. 9 provides examples of the surface topographies of the samples before and after the third series of experimental tests for each tool, along with selected roughness parameters.

The adopted set of lapping parameters and printed tools made of PA2200 polyamide powder enabled a significant improvement in the surface quality of Al_2O_3 samples, which was confirmed by the presented surface topographies. For example, the initial values of the height parameters before the lapping process of Sa = 1.84 μm, Sq = 2.24 μm, respectively, were reduced to Sa = 0.83 μm, Sq = 1.09 μm after the third series of experimental tests using tool no. 1 (total time of machining: 120 min). This demonstrates a significant reduction in the initial irregularities occurring on the surface of the test samples. Simultaneously, the extension of machining time in the case of tool no. 2 (total time of machining: 600 min) resulted in a further, but already much smaller decrease in the values of roughness parameters to the level of Sa = 0.64 μm, Sq = 0.96 μm, which was probably due to the characteristic porous structure of the lapped technical ceramics. The lapping process of hard technical ceramics was also characterized by relatively high efficiency. The total mass material loss of Al_2O_3 samples for tool no. 1 was Δm = 12.13 g after 360 min of lapping, while for tool no. 2 it amounted to Δm = 18.43 g after 840 min. Effective machining after long-lasting lapping indicates durable embedment of grains in the active surface of the tools after the transition from three-to two-body abrasion. The obtained technological results confirmed the great potential of SLS-printed lapping tools in the machining of hard and brittle technical ceramics.

Table 5
Straightness deviations of a flat surface of the lapping plate using *LSQ* and *CLRS* method.

Tool number	Condition of the flat surface of the tool	The value of coefficients from the reference line		R^2	Straightness deviations [mm]	
		a	*b*		ΔD_{LSQ}	ΔD_{CLRS}
Lapping wheel no. 1	before experimental tests	−0.0015	0.0849	0.9939	0.013	0.011
	after series 1 (120 min)	−0.0013	0.0494	0.9132	0.061	0.056
	after series 2 (240 min)	−0.0008	0.0274	0.7829	0.071	0.064
	after series 3 (360 min)	−0.0007	−0.0004	0.5504	0.095	0.090
Lapping wheel no. 2	before experimental tests	−0.001	0.1052	0.7342	0.062	0.016
	after series 1 (120 min)	−0.001	0.1103	0.6954	0.077	0.051
	after series 2 (240 min)	−0.001	0.1062	0.6661	0.082	0.076
	after series 3 (840 min)	−0.0002	0.004	0.0907	0.095	0.095

a)

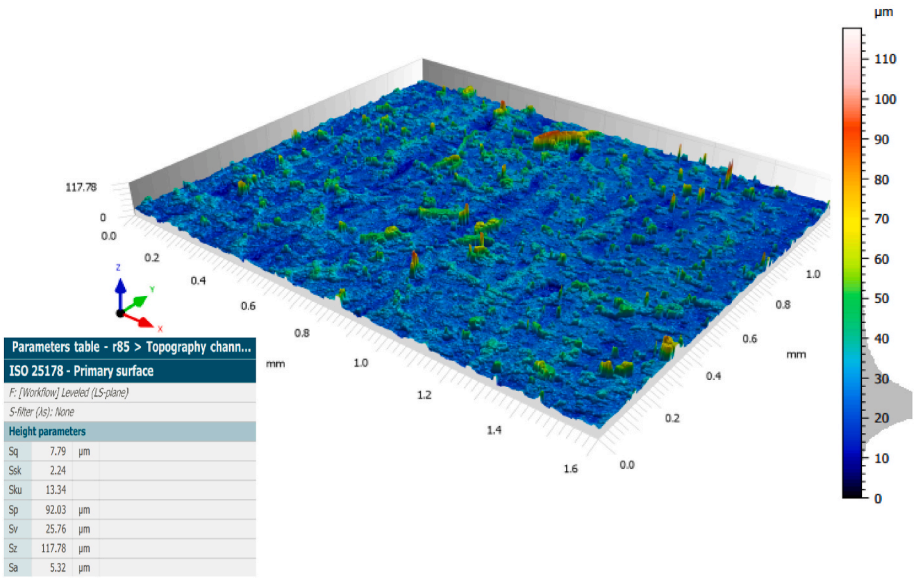

Parameters table - r85 > Topography chann...		
ISO 25178 - Primary surface		
F: [Workflow] Leveled (LS-plane)		
S-filter (λs): None		
Height parameters		
Sq	7.79	µm
Ssk	2.24	
Sku	13.34	
Sp	92.03	µm
Sv	25.76	µm
Sz	117.78	µm
Sa	5.32	µm

b)

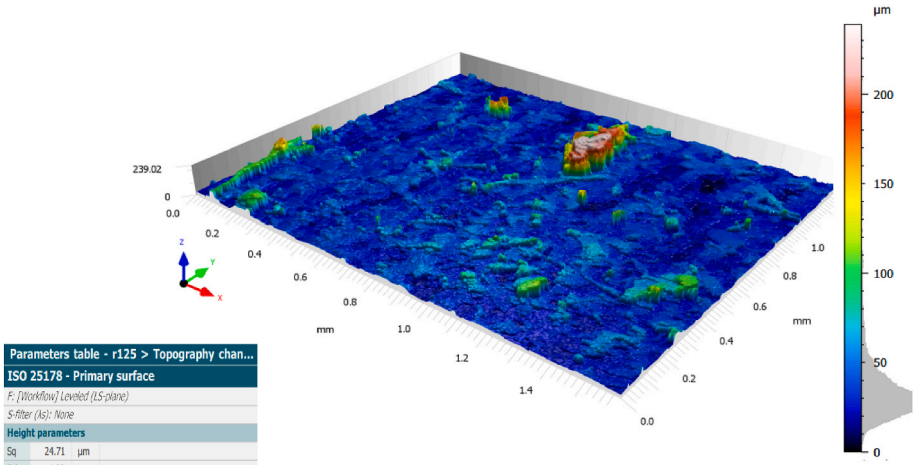

Parameters table - r125 > Topography chan...		
ISO 25178 - Primary surface		
F: [Workflow] Leveled (LS-plane)		
S-filter (λs): None		
Height parameters		
Sq	24.71	µm
Ssk	4.22	
Sku	26.86	
Sp	202.67	µm
Sv	36.36	µm
Sz	239.02	µm
Sa	13.79	µm

c)

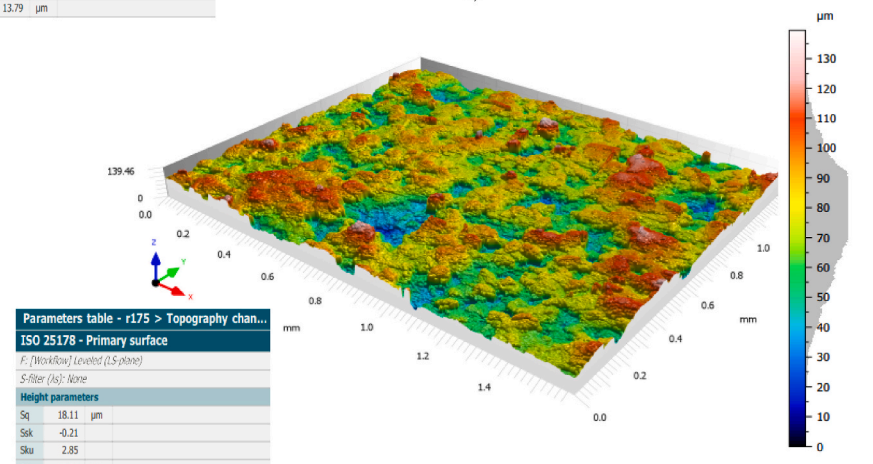

Parameters table - r175 > Topography chan...		
ISO 25178 - Primary surface		
F: [Workflow] Leveled (LS-plane)		
S-filter (λs): None		
Height parameters		
Sq	18.11	µm
Ssk	-0.21	
Sku	2.85	
Sp	63.86	µm
Sv	75.60	µm
Sz	139.46	µm
Sa	14.47	µm

Fig. 7. Three dimensional representation of surface topography of an exemplary lapping segment (# 3) in the measuring radius of: a) 85 mm, b) 125 mm, c) 175 mm.

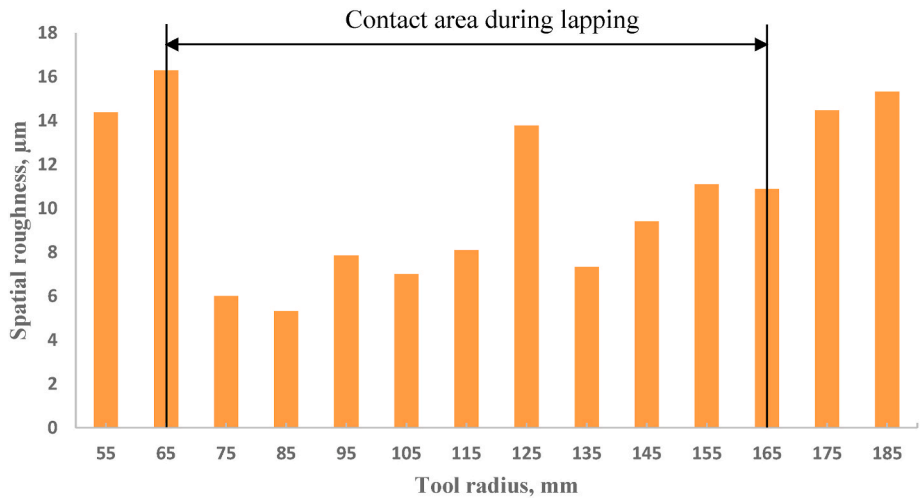

Fig. 8. Spatial roughness (Sa) of an exemplary lapping segment (#3) as a function of radius.

5.4. Discussion

The comparison of 3D printed abrasive tools with conventional material can involve a few aspects, as presented in [54]. In terms of manufacturing cost and productivity, 3D printed polyamide lapping plate shows significant advantages over conventional plates for small batch production. Additionally, 3D printing technology allows the fabrication of complex geometries that are difficult or impossible to produce using conventional machining methods. Fabrication process is simpler and requires the use of significantly less equipment and additional methods as post-processing, reducing the overall production cost. SLS technology is used to fabricate lapping tools through a layer-by-layer sintering process, and the printed parts become unique in their microstructure, depending on the volumetric energy density (VED). However, conventional lapping tools are mostly made from bonded abrasive materials and cast iron, which are homogenous in structure. The fabrication of lapping tools using AM techniques, particularly SLS technology, is seen as a new research topic that offered the potential for custom design fabrication and the benefits of enhancing surface properties while maximising tool performance. A characteristic feature of SLS-printed parts is the internal porous structure, which can have a positive impact on the process and technological results, e.g. through the effective reinforcement of the active surface by abrasive grains without supplying continuously. This embedment could be considered as an advantage for the short machining time, offering faster removal of material. Furthermore, the wear rate of printed tools reported in this research is similar to the wear of conventional cast iron discs as demonstrated in [25], although the latter are much harder. On the other hand, some defects may occur during the 3D printing process, such as warping, micro-cracks, and voids, with lower reproducibility of complex geometrical features, which was not the case for tools tested. SLS-printed tools were used as prototype tools, and therefore experimental data are limited, requiring further study.

VED is an important parameter characterising laser bed fusion techniques, such as SLM and SLS methods. Most polyamide powders were printed at very low laser power, which is less than 30 W and with a very fast printing speeds up to 3467 mm/s [55,56]. However, up to a certain VED value, it is anticipated that a lower scan speed (a higher VED value) will result in the printing of parts with a better mechanical performance. Past this VED value, all of the powder particles will melt, resulting in surface imperfections and more roughness, which lowers the surface quality as shown in [57] also for 3-D printed metals. Generally, there are no suggested or recommended printing parameters to fabricate lapping tools from polyamide powders utilizing SLS technology. As presented in this study, the resulted VED value for the applied laser power of 30 W and printing speed of 10 mm/s was appropriate to produce abrasive segments with the assumed dimensions.

AM-fabricated lapping tools conquer unique microstructures due to the nature of layer-by-layer fabrication. This can lead to different porosity levels and hardness resulting in a potential non-homogeneous structure while influencing the wear behaviour. Due to this, conventional lapping tools can have more predictable wear pattern when compared to the AM-fabricated lapping tool. Those conventional lapping tools are well known because of their great mechanical properties of hardness and toughness, leading to resistance to wear, and the properties of tools from AM can be varied because of their printing parameters such as printing speed, laser power, and layer thickness. This can influence the hardness, toughness, and wear resistance while compared to conventional tools. The wear mechanism is very different for the lapping tools having two body or three body interactions. For the first one, the workpiece interacts only with the lapping plate with embedded abrasive particles, and in the second one, the workpiece, plate, and abrasive particles interact with each other because of the free abrasive particles movement and rotations. This was confirmed by the topographies of the tool's active surface (Fig. 7) and workpieces (Fig. 9), as well as by the differences in the roughness of the tool along its radius (Fig. 8). Even though, during the three-body interaction, conventional lapping plates have a different wear mechanism than AM tools, since the tool fabricated by SLS technology is soft allowing the easier embedment of abrasive particles into the surface of lapping tool during the processing. This influenced the transition of the process from three-to two-body abrasion resulting in effective machining even after 840 min. Considering the above, it seems that abrasive tools fabricated by SLS process are promising for the development and application of lapping technology in the industrial conditions.

6. Conclusions

Experiments were conducted to study the wear characteristic of SLS-printed polyamide PA2200 abrasive tool in single-sided flat lapping of a difficult to cut material Al_2O_3 ceramic. The straightness error of the tool was evaluated by employing the least-squares method *LSQ* and control line rotation scheme *CLRS*, and the analysis of the results allowed drawing the following, most important conclusions.

- The developed prototype tool made using the SLS method was characterized by a relatively low wear value when machining hard and brittle Al_2O_3 technical ceramics.
- The lapping tool surface topography was analyzed after machining ceramic material for 840 min and resulted with indicating the

a)

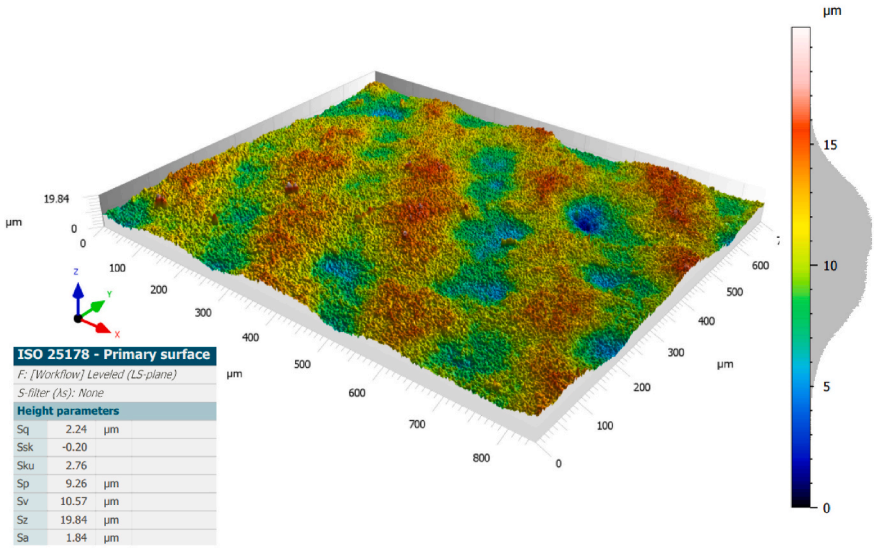

b)

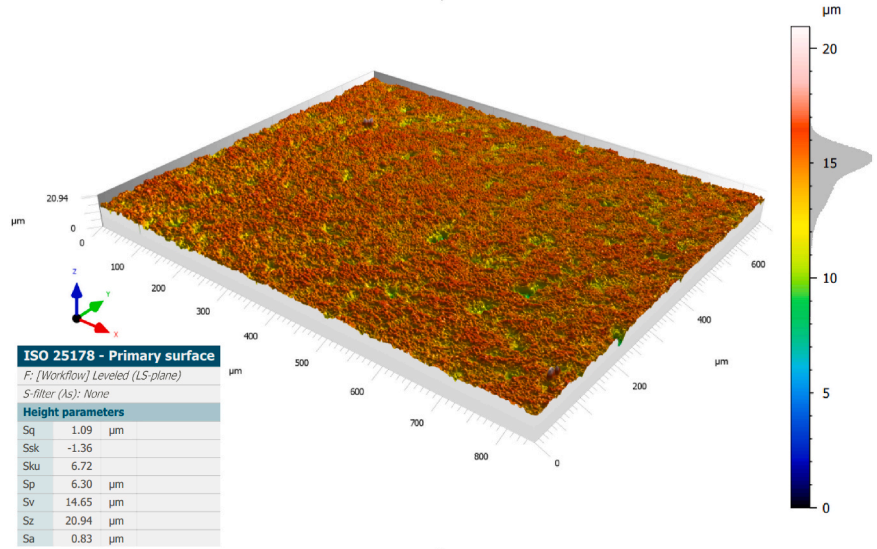

c)

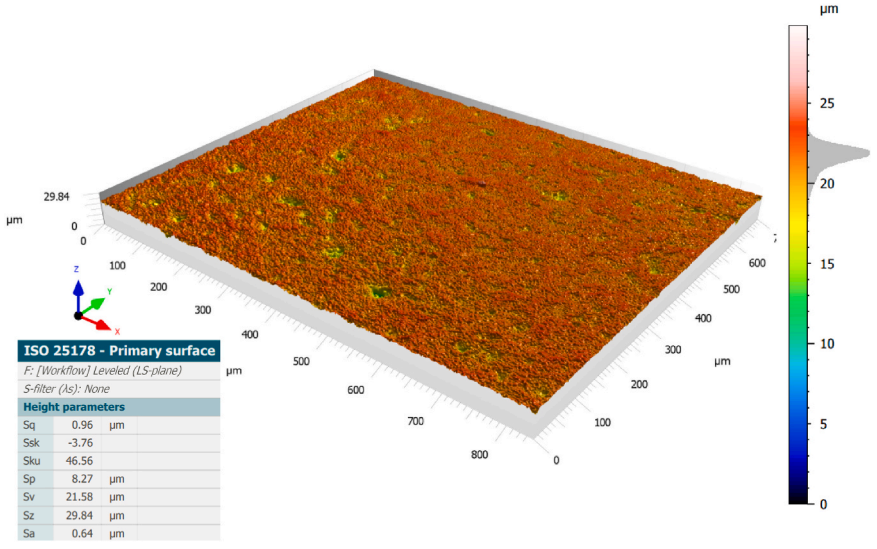

Fig. 9. Surface topographies of the Al_2O_3 samples with selected height parameters: a) initial state (before machining), b) after series 3 of machining with tool no. 1, c) after series 3 of machining with tool no. 2.

highest contact zone of the tool-workpiece, which is in the range of tool radius of 75 mm ÷ 105 mm. The lowest spatial roughness is located at radius of 85 mm with the value of Sa = 5.32 μm and this location is expected as a bigger wear location on the lapping tool.

- The adopted set of process parameters allowed a significant smoothing of the machined ceramic surface and a decrease in the values of roughness parameters from the initial level of Sa = 1.84 μm, Sq = 2.24 μm to the values of Sa = 0.64 μm, Sq = 0.96 μm after 600 min of lapping.
- SLS printed polyamide PA2200 abrasive tool has shown the effectiveness during lapping hard and brittle ceramic material Al_2O_3 samples. The technological result indicated 12.13 g of mass loos of the sample after 360 min of lapping by tool no.1 and 18.43 g mass loss of the sample after 840 min lapping of the sample.

Overall, considerable advancements in the machinability of ceramic materials have been shown by the use of the selectively laser sintered (SLS) printed polyamide PA2200 abrasive lapping tool in single-sided lapping operations. Analysis of straightness error and tool wear demonstrated the area where a significant wear is located in the lapping tool, with the SLS-printed tool showing good material removal and comparatively low wear rates. Experimental observations confirmed the results from the simulations revealing that the lapping tool's near-inner radius had the highest wear, which is noteworthy and offers important information for future tool design improvements. Further investigation of various kinematic parameters could offer insightful information about optimizing the machinability of Al_2O_3 ceramic materials while taking the uniformity of tool wear into consideration, and this will incorporate to the ongoing advances in precision manufacturing processes. Further study of the impact of VED on the mechanical and surface properties of the printed polyamide lapping tools will be also conducted.

Funding

This work is funded by the European Commission in the framework HORIZON-WIDERA-2021-ACCESS-03, project 101079398 'New Approach to Innovative Technologies in Manufacturing (NEPTUN)', https://doi.org/10.3030/101079398

CRediT authorship contribution statement

Mariusz Deja: Writing – review & editing, Visualization, Software, Methodology, Formal analysis, Conceptualization, Data curation, Funding acquisition, Project administration, Resources, Supervision, Validation. **Dawid Zieliński:** Writing – original draft, Validation, Methodology, Investigation, Formal analysis, Conceptualization, Data curation, Resources, Software, Supervision, Visualization, Writing – review & editing. **Sisay Workineh Agebo:** Writing – review & editing, Writing – original draft, Validation, Software, Methodology, Investigation, Data curation, Conceptualization, Formal analysis, Resources, Supervision, Visualization.

Declaration of competing interest

The authors declare that they have no known competing financial interests or personal relationships that could have appeared to influence the work reported in this paper.

Data availability

Data will be made available on request.

Acknowledgements

Computations carried out with the use of the software and computers from Academic Computer Center in Gdańsk, Poland - TASK (http://www.task.gda.pl).

References

[1] C. Park, H. Kim, S. Lee, H. Jeong, The influence of abrasive size on high-pressure chemical mechanical polishing of sapphire wafer, Int. J. of Prec. Eng. and Manu.-G. Tech. 2 (2) (2015) 157–162.
[2] Y. Tian, et al., Effects of chemical slurries on fixed abrasive chemical-mechanical polishing of optical silicon substrates, Int. J. Precis. Eng. Manuf. 14 (8) (2013) 1447–1454.
[3] S. Bhagavat, J.C. Liberato, C. Chung, I. Kao, Effects of mixed abrasive grits in slurries on free abrasive machining (FAM) processes, Int. J. Mach. Tool Manufact. 50 (9) (2010) 843–847.
[4] T. Lee, et al., Effect of platen shape on evolution of total thickness variation in single-sided lapping of sapphire wafer, Int. J. of Prec. Eng. and Manu.-G. Tech. 3 (3) (2016) 225–229.
[5] A. Barylski, M. Deja, Wear of the tool in double-disc lapping of silicon wafers, ASME 2010 Int. Manu. Sci. and Eng. Conf. 1 (2010) 301–307, https://doi.org/10.1115/MSEC2010-34323.
[6] D. Ravimal, et al., Image-based inspection technique of a machined metal surface for an unmanned lapping process, Int. J. of Precis. Eng. and Manuf.-Green Tech. 7 (2020) 547–557, https://doi.org/10.1007/s40684-019-00181-7.
[7] K. Żak, W. Grzesik, Metrological aspects of surface topographies produced by different machining operations regarding their potential functionality, Metrol. Meas. Syst. 24 (2) (2017) 325–335.
[8] Z.C. Li, et al., Simultaneous double side grinding of silicon wafers: a literature review, Int. J. of Ma. To. and Manu. 46 (12–13) (2006) 1449–1458.
[9] M. Deja, D. Zieliński, Wear of electroplated diamond tools in lap-grinding of Al_2O_3 ceramic materials, Wear 460 (2020) 203461.
[10] M. Deja, The use of Preston equation to determine material removal during lap-grinding with electroplated CBN tools, Wear 528 (2023) 204968.
[11] D.J. Moon, et al., Removal mechanisms of glass and sapphire materials by slurry free lapping, in: International Conference on Planarization/CMP Technology, 2015, pp. 1–4.
[12] S. Li, Z. Wang, Y. Wu, Relationship between subsurface damage and surface roughness of optical materials in grinding and lapping processes, J. Mater. Process. Technol. 205 (1–3) (2008) 34–41.
[13] J.B. Wang, et al., Process optimization of lapping sapphire substrate with fixed diamond abrasive pad, Key Engineering Materials Trans Tech Publications Ltd 693 (2016) 1090–1097.
[14] Z. Li, et al., Spectral analysis of surface roughness and form profile of a machined surface after low pressure lapping, Proc. IME B J. Eng. Manufact. 230 (8) (2016) 1399–1405.
[15] A. Barylski, N. Piotrowski, Modeling of lapping plate wear and conditioning in single-sided lapping, in: XXIII International Symposium, Research-Education-Technology, 2017, pp. 1–5.
[16] C.J. Evans, et al., Material removal mechanisms in lapping and polishing, CIRP Ann. - Manuf. Technol. 52 (2) (2003) 611–633.
[17] A. Deaconescu, T. Deaconescu, Robust design of lapping processes, International Conference of DAAAM Baltic Industrial Engineering 1 (2008) 221–226.
[18] A. Deaconescu, T. Deaconescu, Experimental and statistical parametric optimisation of surface roughness and machining productivity by lapping, Trans. FAMENA 39 (4) (2015) 65–78.
[19] Y. Jiandong, et al., Lapping pressure automatically controlling method in high speed lapping, International Conference on Intelligent Computation Technology and Automation 2 (2010) 585–588.
[20] Y. Jiandong, et al., A new method of controlling lapping speed in high speed lapping machine, International Conference on Computer, Mechatronics, Control and Electronic Engineering 1 (2010) 97–100.
[21] Q.J. Zhang, et al., Computer simulation technology of lapping process for polycrystalline diamond, International Conference on Digital Manufacturing & Automation (2012) 289–292.
[22] A.W. Stähli, The Technique of Lapping. Switzerland: Pieterlen/Biel, 2013. https://www.stahliusa.com/wordpress/wpcontent/uploads/2016/06/The_Technique_of_Lapping.pdf. (Accessed 19 January 2024).
[23] L. Sanchez, et al., Surface finishing of flat pieces when submitted to lapping kinematics on abrasive disc dressed under several overlap factors, Precis. Eng. 35 (2) (2011) 355–363.
[24] J.L. Yuan, et al., Research and Simulation on the Wear Uniformity of Lapping Plate, vol. 364, Key Engineering Materials Trans Tech Publications Ltd, 2008, pp. 466–469.
[25] A. Barylski, N. Piotrowski, Non-conventional approach in single-sided lapping process: kinematic analysis and parameters optimization, Int. J. Adv. Manuf. Technol. 100 (1–4) (2019) 589–598.
[26] A. Barylski, M. Deja, Shaping of the workpiece surface in single-disc lapping, Arch. Civ. Mech. Eng. 2 (2) (2002) 5–23.
[27] E. Uhlmann, T. Hoghé, M. Kleinschnitker, Grinding wheel wear prediction at double face grinding with planetary kinematics using analytic simulation, Int. J. Adv. Manuf. Technol. 69 (9–12) (2013) 2315–2321.

[28] E. Uhlmann, T. Hoghé, Wear reduction at double face grinding with planetary kinematics, J. Inst. Eng. Prod. 6 (3) (2012) 237–242.
[29] Z. Lai, et al., Study on the wear characteristics of a lapping wheel in double-sided lapping based on the trajectory distribution, IEEE Trans. Semicond. Manuf. 32 (3) (2019) 352–358.
[30] L. Wang, et al., Study on the double-sided grinding of sapphire substrates with the trajectory method, Precis. Eng. 51 (2018) 308–318.
[31] J. Yuan, et al., Kinematics and trajectory of both-sides cylindrical lapping process in planetary motion type, Int. J. of Mac. To. and Manu. 92 (2015) 60–71.
[32] J. Kling, E. Matthias, Workpiece material removal and lapping wheel wear in plane and plane-parallel lapping, CIRP Annals 35 (1) (1986) 219–222.
[33] Q. Huang, L. Guo, I.D. Marinescu, Grind/lap of Ceramics with Uv-Bonded Diamond Wheels, Handbook of Ceramics Grinding and Polishing Second Edi, 2015, pp. 360–393, https://doi.org/10.1016/b978-1-4557-7858-4.00010-8.
[34] I. Marinescu, L. Guo, P. Wei, Basic research for the uv fixed abrasive lapping plate, Appl. Mech. Mater. 371 (2013) 95–100.
[35] W.B. Williams, Additive Manufacturing of Tools for Lapping Glass, 8884, Optifab 2013 International Society for Optics and Photonics, 2013, p. 88840M, https://doi.org/10.1117/12.2028699.
[36] T. Tanaka, Y. Isono, New development of a grinding wheel with resin cured by ultraviolet light, J. Mater. Process. Technol. 113 (1–3) (2001) 385–391, https://doi.org/10.1016/S0924-0136(01)00636-7.
[37] M. Deja, et al., Application of rapid prototyping technology in the manufacturing of turbine blade with small diameter holes, Pol. Marit. Res. 25 (1) (2018) 119–123, https://doi.org/10.2478/pomr-2018-0032.
[38] M. Deja, D. Zielinski, A pilot study to assess an in-process inspection method for small diameter holes produced by direct metal laser sintering, Rapid Prototyp. J. 26 (2) (2019) 418–436, https://doi.org/10.1108/RPJ-05-2019-0132.
[39] A. Gebhardt, Understanding Additive Manufacturing, Carl Hanser Verlag GmbH & Co. KG, 2011, pp. I–IX, https://doi.org/10.3139/9783446431621.fm.
[40] L. Guo, et al., An experimental study on the abrasive machining process of electronic substrate material with a novel ultraviolet-curable resin bond diamond lapping plate, IEEE Access 7 (2019) 64375–64385.
[41] L. Guo, et al., An experimental study on the precision abrasive machining process of hard and brittle materials with ultraviolet-resin bond diamond abrasive tools, Materials 12 (1) (2019) 125.
[42] W.B. Williams, The Impact of Layer Thickness on the Performance of Additively Manufactured Lapping Tools, vol. 9633, Optifab International Society for Optics and Photonics 1–8, 2015 963304, https://doi.org/10.1117/12.2195995.
[43] M. Deja, D. Zielinski, A Pilot Study on machining difficult-to-cut materials with the use of tools fabricated by SLS technology, Materials 14 (2021) 5306, https://doi.org/10.3390/ma14185306.
[44] K.R. Muratov, et al., Study of lapping and polishing performance on lithium niobate single crystals, Materials 14 (2021) 4968, https://doi.org/10.3390/ma14174968.
[45] N. Macerol, et al., A lapping-based test method to investigate wear behaviour of bonded-abrasive tools, CIRP Ann. - Manuf. Technol. 71 (1) (2022) 305–308, https://doi.org/10.1016/j.cirp.2022.04.049.
[46] Z. Wang, et al., Comparison of lapping performance between fixed agglomerated diamond pad and fixed single crystal diamond pad, Wear 432–433 (2019) 202963, https://doi.org/10.1016/j.wear.2019.202963.
[47] J. Chen, et al., A novel agglomerated diamond abrasive with excellent micro-cutting and self-sharpening capabilities in fixed abrasive lapping processes, 44-465, Wear (2020) 203531, https://doi.org/10.1016/j.wear.2020.203531.
[48] Q. Xiong, et al., Processing performance of vitrified bonded fixed - abrasive lapping plates for sapphire wafers, Int. J. Adv. Manuf. Technol. (2022) 1945–1955, https://doi.org/10.1007/s00170-022-10294-0.
[49] H. Kim, et al., Comparison between sapphire lapping processes using 2-body and 3-body modes as a function of diamond abrasive size, Wear 332–333 (2015) 794–799, https://doi.org/10.1016/j.wear.2015.02.029.
[50] Z. Lai, et al., Study on the wear characteristics of a lapping wheel in double-sided lapping based on the trajectory distribution, IEEE Trans. Semicond. Manuf. 32 (3) (2019) 352–358, https://doi.org/10.1109/TSM.2019.2912454.
[51] L. Bin, et al., Theoretical and experimental analysis of material removal and surface generation in novel fixed abrasive lapping of optical surface, J. Mater. Process. Technol. (2020) 279, https://doi.org/10.1016/j.jmatprotec.2019.116570.
[52] EOS GmbH *PA 2200 Balance 1.0 PA 12*, 2010. Web site, https://drukarki3d.pl/wp-content/uploads/2015/09/karta-materiałowa-PA-2200-ENG.pdf. (Accessed 12 June 2024).
[53] S.T. Huang, K.C. Fan, J.H. Wu, A new minimum zone method for evaluating straightness errors, Precis. Eng. 15 (3) (1993) 158–165.
[54] M. Deja, D. Zieliński, A.Z.A. Kadir, S.N. Humaira, Applications of additively manufactured tools in abrasive machining—a literature review, Materials 14 (5) (2021) 1318.
[55] Emmanouil L. Papazoglou, et al., The influence of volumetric energy density on the mechanical behavior of PA12 parts produced by Powder Bed Fusion: an experimental and numerical study, Simulat. Model. Pract. Theor. 130 (2024) 102862, https://doi.org/10.1016/j.simpat.2023.102862.
[56] I.M. Kusoglu, et al., Laser powder bed fusion of polymers: quantitative research direction indices, Materials 14 (2021) 1169, https://doi.org/10.3390/ma14051169.
[57] E.M. Pechlivani, et al., On the effect of volumetric energy density on the characteristics of 3D-Printed metals and alloys, Metals 13 (2023) 1776, https://doi.org/10.3390/met13101776.